EXPERIMENTAL FRACTURE DYNAMICS

J.F. Kalthoff

Experimental Mechanics
Ruhr-University Bochum
44780 Bochum, Germany

Resumen. En este trabajo se investigan los efectos transitorios de los procesos de fractura dinámica. Se determina el factor de intensidad de tensiones dinámico utilizando el método óptico de las cáusticas, cuyo principio físico y análisis matemático se describen en este artículo. Para el proceso de propagación de fisuras y su posterior detención, se ha determinado que la condición tensional en el momento de la detención, cuando la velocidad de propagación de la fisura es cero, no es estática sino aún dinámica. Para fisuras bajo cargas de impacto, los factores de intensidad de tensiones pueden llegar a ser erróneos si se hallan a partir de valores externos de carga por medio del factor de intensidad de tensiones estático. La correcta determinación de la tenacidad a fractura requiere procedimientos enteramente dinámicos.

Abstract. Transient effects of dynamic fracture processes are investigated. By the shadow optical method of caustics actual dynamic stress intensity factors are measured. Physical principle and mathematical analysis of the method are described. For the process of propagating and subsequently arresting cracks it is found that the stress condition at the moment of arrest, when the crack velocity has become zero already, is not static but still dynamic. For cracks under impact loading stress intensity factors can become erroneous when determined from external load values via static stress intensity factor relationships. A correct determination of the fracture toughnesses requires fully dynamic procedures.

1. INTRODUCTION

When static fracture toughnesses are determined two parameters are involved: length and force. The measurement of dynamic fracture toughnesses requires the consideration of the additional parameter time. Influences of time on the material behaviour are to be measured, but the parameter time can also have an influence on the measuring procedure itself. In general, engineering measuring procedures in fracture dynamics have their roots in procedures for measuring the equivalent static quantities. Often, the static procedures are directly transferred to the dynamic cases without any changes or with only slight modifications. Such procedures based on quasistatic analyses are easy to apply, but they impose restrictions on the test parameters and limitations on the applicability range of the test. Fully dynamic procedures, on the other hand, give reliable results under arbitrary test conditions but they are necessarily more complicated than static ones.

This paper summarizes work carried out by the author and his colleagues to investigate the influences of dynamic effects on test procedures for measuring dynamic fracture toughnesses: as examples are considered the crack arrest toughness K_{Ia} and the impact fracture toughness K_{Id}. The dynamic influences are quantified by comparing the actual dynamic reactions at the crack tip with the equivalent static behaviour. Conditions are specified under which quasistatic measuring procedures can be applied with sufficient accuracy and where dynamic procedures are needed which take inertial and kinetic effects into account.

The dynamic crack tip reactions are investigated by means of the shadow optical method of caustics. This method is described first and results on the dynamic fracture processes considered are presented in the following sections.

2. THE SHADOW OPTICAL METHOD OF CAUSTICS

Stresses alter the optical properties of a solid, i.e. the thickness of the body (due to Poisson's effects) and the refractive index of the material. These changes in the

optical properties are utilized in the shadow optical method of caustics to make stress concentrations in the solid visible. The method was originally introduced by Manogg [1] in 1964.

2.1 General Considerations

The physical principle of the method is illustrated in Fig. 1. A specimen with a notch or a crack as a stress riser is subjected to tensile loading. The specimen shall be of a transparent material for the moment. It is illuminated by a parallel light beam. Due to the tensile stress concentration around the crack tip the thickness of the specimen and the refractive index of the material are reduced, the reductions are the larger the nearer the

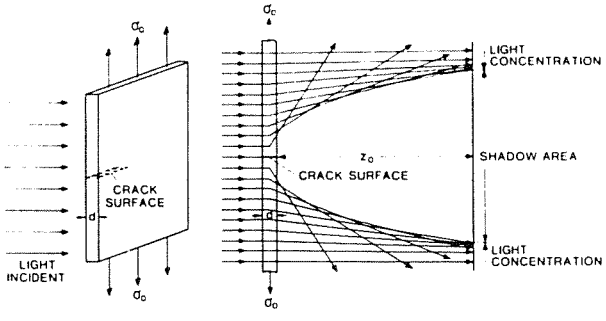

Fig. 1. Physical principle of the shadow optical method of caustics

considered area to the crack tip. Thus, a light ray traversing the specimen in the neighbourhood of the crack tip is deflected in a direction away from the crack tip. With that respect the area surrounding the crack tip acts similar to a divergent lens. But, the closer the light ray to the crack tip the larger the deflection angle. Consequently, on a screen (image or reference plane) at a distance z_0 from the specimen, the crack tip appears as a shadow area which is surrounded by a region of light concentration. The boundary line between the shadow area and the area of light concentration is the caustic. The shadow pattern, more precisely the caustic, represents a quantitative description of the stress intensification at the crack tip.

Shadow optical light patterns are obtained for tensile as well as compressive stress concentrations (in the latter case for notches only). They can be observed with transparent specimens or in reflection with non-transparent specimens, as real or as virtual images. Figure 1 represents the most simple case of a tensile stress concentration in a transparent specimen with the observation of a real shadow optical image. The virtual image is obtained on the opposite side of the specimen where the real image is observed. In reflection, the light rays which are reflected at the front side of the specimen, i.e. the side facing the light source, are considered. These light rays lead to the formation of shadow images as well. Again, they can be real or virtual depending on the position of the image plane.

For the mathematical description of light ray deflections the following sign assignments and definitions are made: Tensile stresses are positive. The observation direction defines the sign of distances. The distance z_0 between the reference plane and the specimen is positive (negative) if the reference plane is located ahead of (behind) the specimen - when looking in observation direction. In transmission (reflection) arrangements the observation direction is opposite to (in) the direction of the illuminating light beam.

2.2 Shadow Optical Mapping Equations

Figure 2 considers the mapping of the object plane E (the specimen) onto a real shadow optical image plane E' for a transmission arrangement, $z_0 > 0$. The given formulas, however, apply quite generally for any observation mode if the appropriate signs of the representative distances are used. A light ray traverses

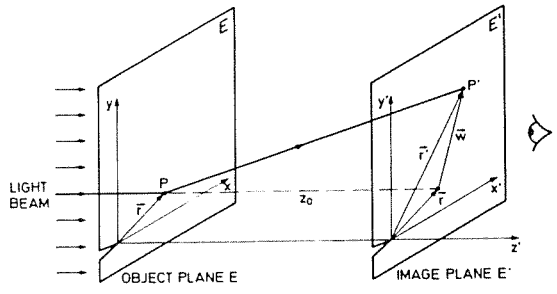

Fig. 2. Mapping of the object plane onto the image plane

the object plane E at the point $P(\vec{r})$, where $\vec{r}$ is the radial distance from the crack tip. Due to the influence of the stresses in the specimen this light ray is deflected and hits the image plane E' displaced by the vector $\vec{w}$ at the point $P'(\vec{r})$ with

$$\vec{r} = \vec{r} + \vec{w}. \qquad (1)$$

Direction and magnitude of the displacement vector $\vec{w}$ are controlled by the change in optical path length which the light ray experiences in the object plane. Figure 3 illustrates the situation for a simplified one-dimensional case. Considered are stresses and light deflections in y-direction only. The planar wavefront of an impinging light beam is distorted when traversing the specimen as a result of changes in the thickness of the plate and in

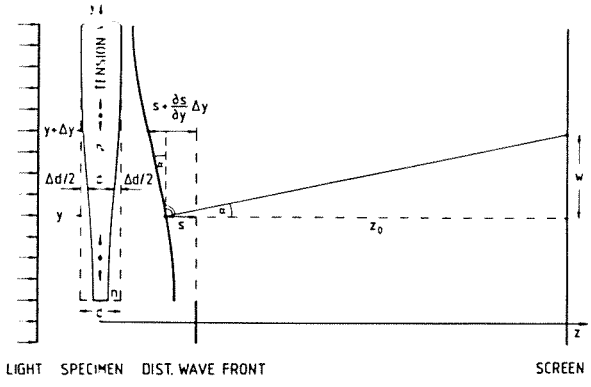

Fig. 3. On the light ray deflection due to stresses in a solid (one-dimensional consideration)

the refractive index of the material. The local retardation of the distorted wavefront, denoted s, with regard to an equivalent wavefront that did not pass through the specimen, is given by

$$s = [n_l(y) - 1]\, d_l(y) \qquad (2)$$

where $n_l(y)$ = local refractive index of the material, and $d_l(y)$ = local thickness of the specimen. Furthermore, $n_l(y) = n + \Delta n(y)$ and $d_l(y) = d + \Delta d(y)$, where n, d = refractive index of the material and thickness of the specimen without load, and Δn, Δd = changes in refractive index and specimen thickness due to the prevaling stresses. As is readily obtained from Fig. 3

$$w = z_0 \left\{ \frac{\partial s(y)}{\partial y} \right\} \qquad (3)$$

and, consequently,

$$w = z_0 \left\{ [n_l(y) - 1] \frac{\partial d_l(y)}{\partial_y} + d_l(y) \frac{\partial n_l(y)}{\partial_y} \right\} \qquad (4)$$

$$= z_0 \frac{\partial}{\partial y} \left\{ [n - 1] \cdot \Delta d(y) + d \cdot \Delta n(y) \right\}. \qquad (5)$$

Thus, for the general two-dimensional case, i.e. a plate in x-y-plane

$$\vec{w} = z_0 \, \text{grad} \left\{ [n - 1] \, \Delta d(x,y) + d \cdot \Delta n\,(x,y) \right\}. \qquad (6)$$

In the generalized form

$$\vec{w} = z_0 \, \text{grad} \left\{ [n - 1] \, \Delta d_{eff} + d_{eff} \cdot \Delta n \right\} \qquad (7)$$

with n = refractive index, $d_{eff} = d$ for transmission,
and n = -1, $d_{eff} = d/2$ for reflection,
(the deformations at the surface of the specimen result from the strains throughout half the thickness of the plate)

this equation applies with $z_0 > 0$ for real images in transmission or reflection and with $z_0 < 0$ for virtual images in transmission or reflection.

Furthermore, changes Δn in the refractive index due to the prevailing principal stresses σ_1, σ_2, σ_3 are described by Maxwell-Neumann's law

$$\Delta n_1 = A\sigma_1 + B(\sigma_2+\sigma_3), \quad \Delta n_2 = A\sigma_2 + B(\sigma_1+\sigma_3) \qquad (8)$$

with $\Delta n_{1/2}$ = changes in refractive index for light polarized in the 1-/2-directions of the principal stresses, and A, B = material constants. For optically isotropic, non-birefringent materials A = B, and for reflection A = B = 0. Changes Δd_{eff} due to the stresses are described by Hooke's law

$$\Delta d_{eff} = \left[\frac{1}{E}\sigma_3 - \frac{\nu}{E}(\sigma_1 + \sigma_2) \right] d_{eff} \qquad (9)$$

with $\sigma_3 = 0$ for plane stress, and $\Delta d_{eff} = 0$ for plane strain. With Eqs. (8) and (9) the Eq. (7) then can be rearranged to

$$\vec{w} = z_0 \; c \; d_{eff} \; \text{grad} \left[(\sigma_1+\sigma_2) \pm \lambda(\sigma_1-\sigma_2) \right] \qquad (10)$$

with

$$c = \frac{A+B}{2} - (n-1)\frac{\nu}{E}, \quad \lambda = \frac{A-B}{A+B-2(n-1)\nu/E} \quad \text{for plane stress}$$

$$c = \frac{A+B}{2} - \nu B, \quad \lambda = \frac{A-B}{A+B+2\nu B} \quad \text{for plane strain.}$$

Numerical values for the constants used in Eqs. (7) - (10), in particular for the shadow optical constant c and the anisotropy coefficient λ, are given for different materials in Table 1.

The complete family of light rays which are deflected according to Eq. (1) with Eq. (10) forms a shadow space behind the object plane (see also Fig. 1). Its surface is an envelope to the light rays and is called the caustic surface. The intersection of this surface with the image plane forms the caustic curve. The caustic is a multivalued, singular solution of the mapping equations, i.e. the mapping of points along the caustic is not reversible. Thus, a necessary and sufficient condition for the existence of the caustic curve is obtained if the Jacobian of Eq. (1) with Eq. (10) becomes zero, i.e.

	Elastic Constants		General Optical Constants			Shadow Optical Constants for Plane Stress		Shadow Optical Constants for Plane Strain		Effective Thickness
Material	Young's Modulus MN/m^2	Poisson's Ratio	Refractive Index	A m^2/N	B m^2/N	c m^2/N	λ	c m^2/N	λ	d_{eff}
TRANSMISSION ($z_0 < 0$)										
Optically Anisotropic										
Araldite B	3660*	0.392*	1.592	-0.056×10^{-10}	-0.620×10^{-10}	-0.970×10^{-10}	-0.288	-0.580×10^{-10}	-0.482	d
CR-39	2580	0.443	1.504	-0.160×10^{-10}	-0.520×10^{-10}	-1.200×10^{-10}	-0.148	-0.560×10^{-10}	-0.317	d
Plate Glass	73900	0.231	1.517	$+0.0032 \times 10^{-10}$	-0.025×10^{-10}	-0.027×10^{-10}	-0.519	-0.017×10^{-10}	-0.849	d
Homalite 100	4820*	0.310*	1.561	-0.444×10^{-10}	-0.672×10^{-10}	-0.920×10^{-10}	-0.121	-0.767×10^{-10}	-0.149	d
Optically Isotropic										
PMMA	3240	0.350	1.491	-0.530×10^{-10}	-0.570×10^{-10}	-1.080×10^{-10}	-0	-0.750×10^{-10}	-0	d
REFLECTION ($z_0 > 0$)										
All materials	E	ν	-1	0	0	2ν/E	0	-	-	d/2

*) dynamic values

Table 1. Constants for caustic evaluation

$$\frac{\partial x'}{\partial r}\frac{\partial y'}{\partial \varphi} - \frac{\partial x'}{\partial \varphi}\frac{\partial y'}{\partial r} = 0 \qquad (11)$$

The coordinates r, φ of points P which fulfill Eq. (11) form the socalled initial curve in the object plane. The mapping of this initial curve onto the image plane is the caustic.

2.3 Mode-I Crack Tip Caustics

With the linear-elastic stress distribution around the tip of a tensile mode-I loaded crack

$$\begin{aligned}\sigma_r &= \frac{K_I}{\sqrt{2\pi r}}\frac{1}{4}\left(5\cos\tfrac{1}{2}\varphi - \cos\tfrac{3}{2}\varphi\right)\\ \sigma_\varphi &= \frac{K_I}{\sqrt{2\pi r}}\frac{1}{4}\left(3\cos\tfrac{1}{2}\varphi + \cos\tfrac{3}{2}\varphi\right)\\ \tau_{r\varphi} &= \frac{K_I}{\sqrt{2\pi r}}\frac{1}{4}\left(\sin\tfrac{1}{2}\varphi + \sin\tfrac{3}{2}\varphi\right)\end{aligned} \qquad (12)$$

where K_I = mode-I stress intensity factor, the mapping equation, i.e. Eq. (1) with Eq. (10), specified for the crack problem and expressed in terms of the components of the vector $\vec{r}$, denoted x' and y', is obtained as

$$\begin{aligned}x' &= r\cos\varphi - \frac{K_I}{\sqrt{2\pi}} z_0\, c\, d_{eff}\, r^{-3/2}\cos\tfrac{3}{2}\varphi\\ y' &= r\sin\varphi - \frac{K_I}{\sqrt{2\pi}} z_0\, c\, d_{eff}\, r^{-3/2}\sin\tfrac{3}{2}\varphi\end{aligned} \qquad (13)$$

For simplicity, only the isotropic case ($\lambda = 0$) is considered in Eq. 13 and throughout the following context. Condition (11) applied to these mapping equations then yields the equation of the initial curve

$$r = \left(\frac{3}{2}\frac{|K_I|}{\sqrt{2\pi}}|z_0|\,|c|d_{eff}\right)^{2/5} \equiv r_0 \ . \qquad (14)$$

The initial curve represents a circle around the crack tip with fixed radius r_0. The caustic curve is finally obtained as the image of the initial curve, given by the equations

$$\begin{aligned}x' &= r_0\left(\cos\varphi - \mathrm{sgn}\,(K_I z_0 c)\tfrac{2}{3}\cos\tfrac{3}{2}\varphi\right)\\ y' &= r_0\left(\sin\varphi - \mathrm{sgn}\,(K_I z_0 c)\tfrac{2}{3}\sin\tfrac{3}{2}\varphi\right) \ .\end{aligned} \qquad (15)$$

The caustic equations are different for different signs of the product $(K_I z_0 c)$. Mathematically, the caustic curves are generalized epicycloids, they are graphically shown in Fig. 4 for different loading conditions, i.e. $K_I > 0$ and $K_I < 0$, different observation modes, i.e. transmission ($c < 0$) and reflection arrangements ($c > 0$, see Table 1), and positive and negative reference distances z_0.

For the quantitative evaluation of caustics a length parameter between characteristic points on the caustic curve is defined. When caustics with an overall negative sign are considered, the maximum diameter of the caustic perpendicular to the crack direction is appropriate, see Fig. 4. This diameter is denoted D. Its

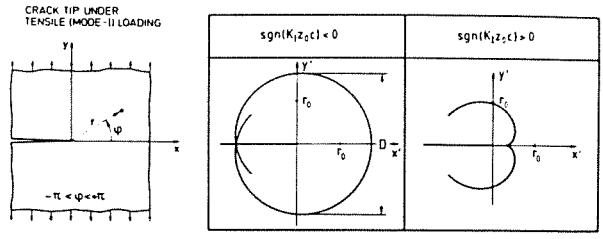

Fig. 4. Crack tip caustics

size is related to the radius of the initial curve by the relationship

$$D = 3.17\, r_0 \qquad (16)$$

With Eq. (14) and (16) a quantitative formula is then obtained relating the size of the shadow pattern to the stress intensity factor K_I

$$|K_I| = \frac{2\sqrt{2\pi}}{3\,(3.17)^{5/2}\,|z_0||c|\,d_{eff}} D^{5/2} \ . \qquad (17)$$

Thus, from the diameter D measured with an experimentally observed caustic the stress intensity factor K_I can quantitatively be determined.

With materials that are optically anisotropic ($\lambda \neq 0$) the analysis becomes somewhat more complex. As a result, the single caustic curve splits up into a double caustic. The evaluation formulas for each of the two caustics are the same as given by Eq. (17) except for slightly different values of the numerical factor. For details see [2].

2.4 Extensions of the Method and Discussion

The presented shadow optical analysis applies for the case of tensile mode-I loaded cracks and linear-elastic material behaviour only. The caustic analysis has been extended to other cases as well. An overview is given by the author in a special chapter of the Handbook on Experimental Mechanics [2]. Some of the results shall be presented.

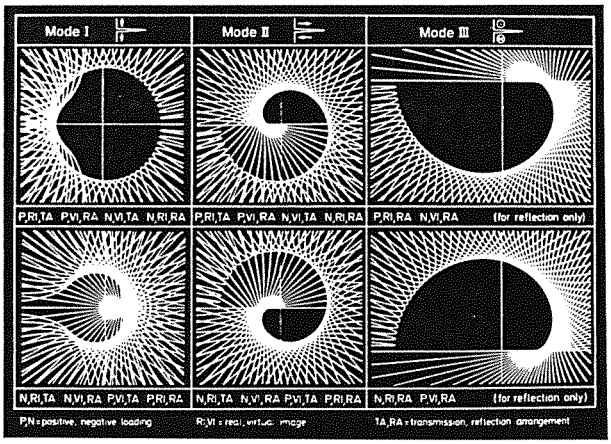

Fig. 5. Crack tip shadow patterns for different modes of loading

Figure 5 shows crack tip shadow patterns for mode-II (in-plane shear) and mode-III (anti-plane shear) loading of cracks, which are shown in addition to the previously derived mode-I caustics. The individual lines in the graphs represent images of light rays which traverse the specimen along straight lines φ = const. The caustic curves appear as envelopes to the obtained families of image lines. The mode-II and the mode-III caustics become asymmetric. As discussed before, a characteristic length parameter of the caustics determines the stress intensity factors K_{II} or K_{III} respectively. For cracks subjected to a combined mode-I mode-II loading both stress intensity factors K_I and K_{II} are determined by two characteristic length parameters taken from the resulting mixed mode caustic. Quantitative formulas are given in [2,3].

With materials that do not show a linear-elastic but an elastic-plastic behaviour (e.g. structural steels) crack tip caustics can be observed as well. Figure 6 shows numerically calculated [4] mode-I shadow patterns of a crack in a power-law hardening material for different hardening exponents n. With increasing influence of plasticity effects the caustic changes its shape from the limiting case n = 1, i.e. a linear-elastic material, to the case n = ∞, i.e. an elastic-perfectly-plastic material. Analogous to the previous discussion, the diameter of the elastic-plastic caustic now determines the elastic-plastic fracture mechanics parameter, i.e. the J-integral. For quantitative formulas see [2,4].

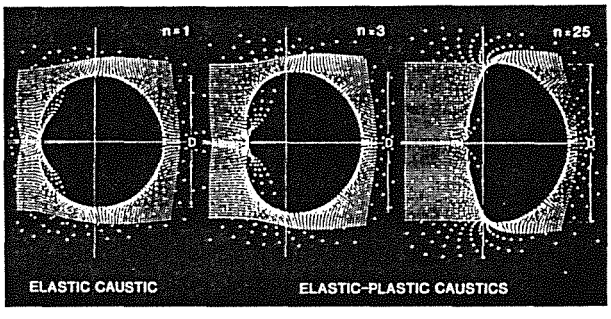

Fig. 6. Elastic-plastic crack tip caustics

For further details, in particular as regards dynamic applications, the influence of higher order terms of the stress distribution and the influence of local plasticity, state of stress, or anisotropy of the material etc., see [2].

Advantages but also shortcomings of the shadow optical technique shall be discussed by comparing the shadow optical and the photoelastic picture of a crack tip stress distribution, Fig. 7. Due to the large number of isochromatic fringes the photoelastic pattern is rather complicated. In the near field region around the crack tip, i.e. the region of interest, the isochromatic fringes are not resolved anymore. Thus, only by extrapolation of far field data towards the center of stress concentration information on the real crack tip loading condition can be obtained. The shadow optical picture, on the other hand, is much simpler. Only one characteristic line, the caustic curve, is obtained which is directly related to the crack tip loading condition. This

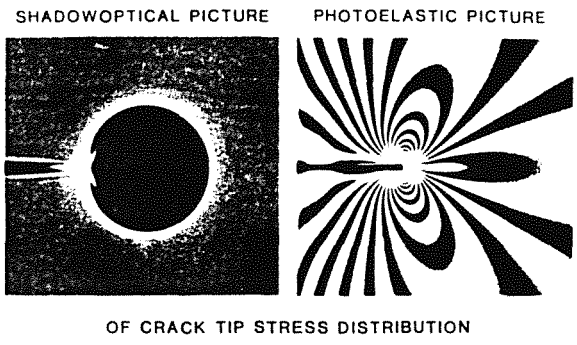

Fig. 7. Shadow optical and photoelastic crack tip patterns

simplicity results from the fact that the shadow optical effect is caused by stress gradients (in contrast to the photoelastic effect caused by stresses). This dependence, on the gradient of stresses, also implies certain disadvantages. The far field of the crack tip stress distribution, for example, does not become visible in the shadow optical picture, since the variations in stresses are too small. The photoelastic pattern, however, yields accurate information in particular in this region. Thus, depending on the specific property of interest and problem to be investigated the shadow optical method of caustics or the photoelastic method of isochromatic fringes (or another experimental method) may be the most appropriate tool of investigation, but, because of its sensitivity to stress gradients the shadow optical method of caustics is certainly advantageous for quantifying the intensification of stresses in the direct vicinity of stress risers.

2.5 Experimental Arrangements

The practical realization of the caustic technique in the laboratory for investigating fracture mechanics problems does not require sophisticated experimental equipment. The only essentials are a suitable light beam for illuminating the specimen and a device for recording the shadow pattern. The light beam has to fulfill only one, but very stringent requirement: it must be generated by a (point-like) light source of very small aperture in order to produce high quality caustics. Conventional cameras can be utilized for the recording of shadow patterns. In dynamic applications a high speed camera is needed. The camera is simply focused onto the real or virtual image plane ahead of or behind the specimen, depending on the chosen observation mode. Despite of the simplicity of the arrangement much care and experimental skill is a prerequisite for successful work. For details on experimental techniques, e.g. specimen preparation, use of non-parallel light beams for illumination of the specimen, quality of the optical set-up etc., see [2].

The patterns that are obtained by the shadow optical method of caustics are of very simple geometrical shape that can easily and reliably be evaluated. The shadow optical method, therefore, is very well suited for investigating complex phenomena, as they apply in

dynamic loading situations. Results of shadow optical investigations of two dynamic fracture problems are presented in the following chapters. In these experiments the dynamic shadow patterns are recorded with a Cranz-Schardin 24 spark high speed camera, allowing minimum picture interval times of 0.5 μs.

3. ARRESTING CRACKS

The usual procedure for measuring the crack arrest toughness K_{Ia} of a material is as follows: In a wedge loaded specimen a rapidly propagating crack is initiated from a blunted initial notch at an initiation stress intensity factor $K_{Iq} > K_{Ic}$. Figure 8 shows a rectangular double cantilever beam specimen under longitudinal wedge loading in a schematic representation. Because of the stiffness of the loading system the crack opening displacement remains constant during crack propagation. Thus, the crack propagates into a decreasing stress intensity factor field. It arrests at the length a_a if the conditions for crack propagation are not

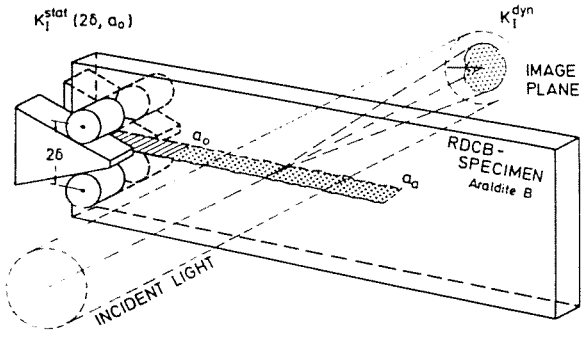

Fig. 8. Experimental set-up for a crack arrest experiment and shadow optical arrangement in transmission (schematically)

fulfilled anymore. To a certain extend, the arrest process is equivalent to an initiation process with the time axis being reversed. The stress intensity factor value at arrest represents the crack arrest toughness K_{Ia}. Recommendations for measuring the arrest toughness are given in ASTM E 1221 [5].

3.1 Influence of Kinetic Effects on the Crack Arrest Process

In order to investigate the influence of dynamic effects on the mechanical behaviour of cracks at arrest, the stress condition at the tip of a propagating and subsequently arresting crack was analyzed, see also [6,7]. Using the epoxy resin Araldite B, the actual dynamic stress intensity factors, K_I^{dyn}, were measured by means of the shadow optical method of caustics in transmission. These values are compared to the equivalent static stress intensity factors, K_I^{stat}, calculated from the measured crack opening displacement 2δ utilizing conventional stress intensity factor formulas from ASTM E 399.

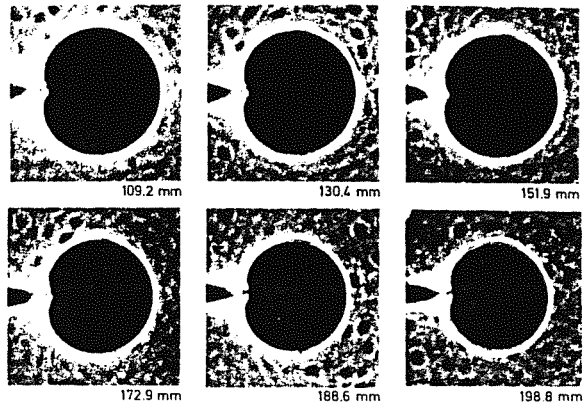

Fig. 9. Caustics of a propagating and subsequently arresting crack (photographed in transmission with an Araldite B specimen)

A series of six shadow optical photographs is shown in Fig. 9. Quantitative data for cracks initiated at different K_{Iq}-values are presented in Fig. 10, showing the dynamic, experimentally determined stress intensity factors, K_I^{dyn}, as a function of crack length together with the corresponding static stress intensity factor curves, $K_I^{stat}(a)$. In addition, the measured crack velocities are given in the lower part of the diagram. The following characteristics of the crack arrest process can be deduced from these results: At the beginning of the crack propagation phase the dynamic stress intensity factor K_I^{dyn} is smaller than the corresponding static value K_I^{stat}. At the end of the propagation phase, in particular at the moment of arrest, the dynamic stress intensity factor K_I^{dyn} is larger than the corresponding

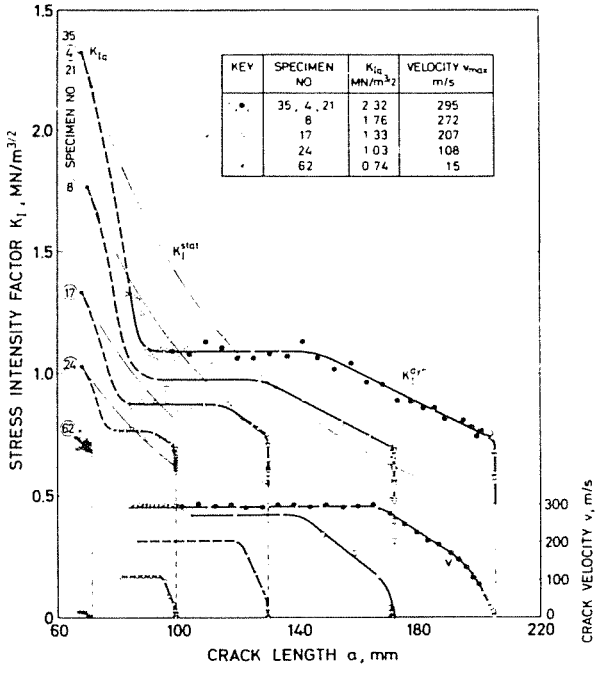

Fig. 10. Stress intensity factors and crack velocity for propagating and subsequently arresting cracks

static value K_I^{stat}. Only after arrest does the dynamic stress intensity factor K_I^{dyn} approach the static stress intensity factor at arrest, K_{Ia}^{stat}. Differences between the dynamic and the static stress intensity factor curves become smaller for cracks initiated at lower K_{Iq} values, i.e. for cracks propagating at lower velocities. The dynamic effects obviously decrease with decreasing velocity, as one might expect.

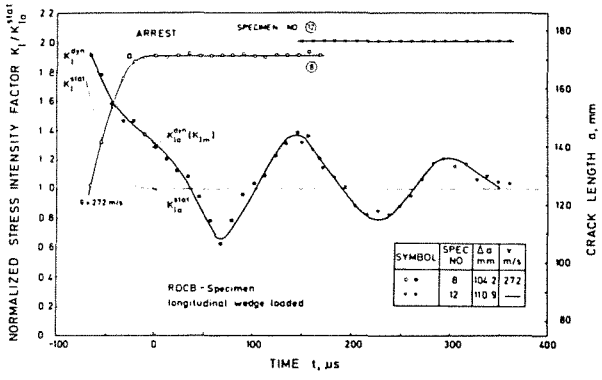

Fig. 11. Post-arrest behaviour

The behaviour of the dynamic stress intensity factor, K_I^{dyn}, in the post-arrest phase is shown in Fig. 11 as a function of time. K_I^{dyn} oscillates around the value of the static stress intensity factor at arrest, K_{Ia}^{stat}. Only some time after arrest does the dynamic stress intensity factor approach the static value.

Wave propagation phenomena explain the observed behaviour: Elastic waves are produced by the propagating crack, so that kinetic energy is radiated into the specimen and $K_I^{dyn} < K_I^{stat}$. After reflection at the finite boundaries of the specimen the waves interact with the crack again and contribute to the stress intensity factor, consequently $K_I^{dyn} > K_I^{stat}$. An illustrative view of these processes is given in Fig. 12. A rapidly propagating crack (1000 m/s) in a high strength steel specimen was photographed in a shadow optical reflection arrangement. In addition to the shadow spot at the crack tip the photograph shows the generation of waves at the tip of the propagating crack and the subsequent reflection at the boundaries of the specimen.

3.2 Influences on the Crack Arrest Toughness K_{Ia}

The observed findings are summarized in Fig. 13. The data show that the stress condition at arrest is not static but dynamic, although the crack velocity is zero at the moment of arrest. Therefore, crack arrest toughness values which are determined on the basis of a static evaluation procedure in principle cannot represent true material properties. Statically determined crack arrest toughness values K_{Ia}^{stat} are smaller than the true dynamically determined crack arrest toughness values K_{Ia}^{dyn}.

The standard ASTM E 1221 [5] for measuring crack arrest toughnesses is based on a static evaluation procedure and care is, therefore, needed in using such toughness data. Safety predictions on the basis of K_{Ia}^{stat} data can be erroneous. The determination of the true crack arrest toughness has to take the dynamic effects

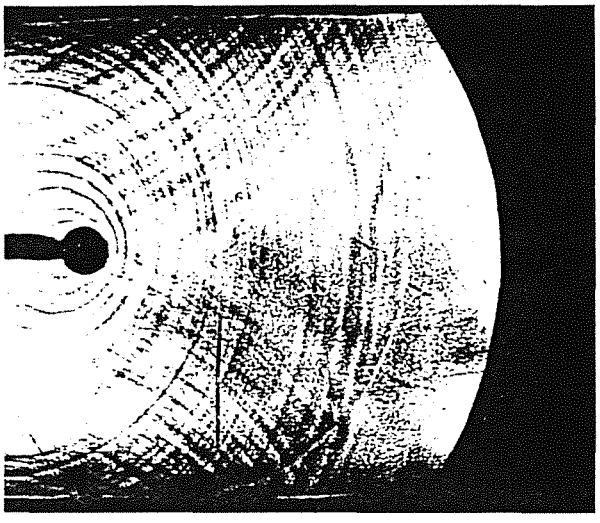

Fig. 12. Shadow optical photograph of a fast propagating crack in steel

into account and requires a fully dynamic analysis. However, since the dynamic effects in large scale structures are generally smaller than in the relatively small laboratory test specimens which are used for K_{Ia} determination, static crack arrest analyses will yield conservative crack arrest predictions [6]. On the basis of this understanding the static crack arrest concept can be applied by the practical engineer under certain circumstances.

In order to minimize the errors when applying the static crack arrest concept a special crack arrest test specimen

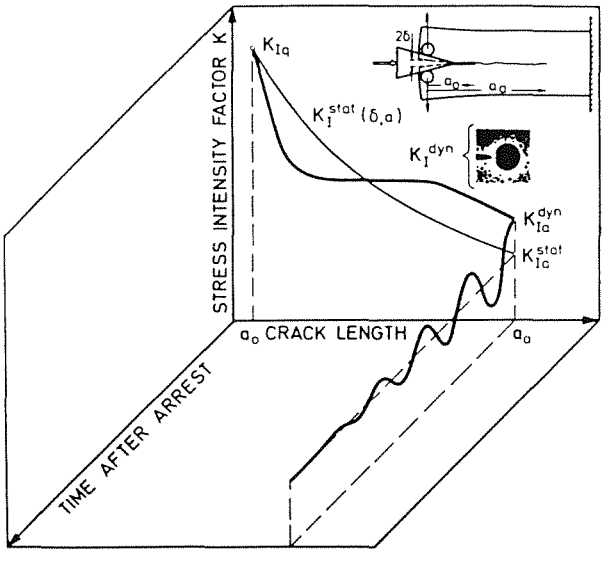

Fig. 13. Crack arrest behaviour (schematically)

with reduced dynamic effects has been developed by the author and his colleagues, the socalled RDE-specimen, [6]. With this specially designed specimens, crack arrest toughness data can be determined by static evaluation procedures with an accuracy which is sufficient for engineering purposes and which avoids over-conservatism.

4. CRACKS UNDER IMPACT LOADING

The impact fracture toughness K_{Id} is usually determined with precracked bend specimens in instrumented impact tests. The specimen is loaded by a drop weight or by a pendulum type impact testor. Strain gauges at the tup of

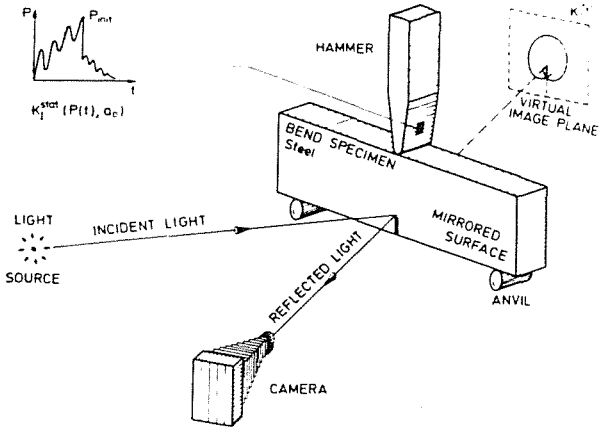

Fig. 14. Experimental set-up for a drop weight experiment and shadow optical arrangement in reflection (schematically)

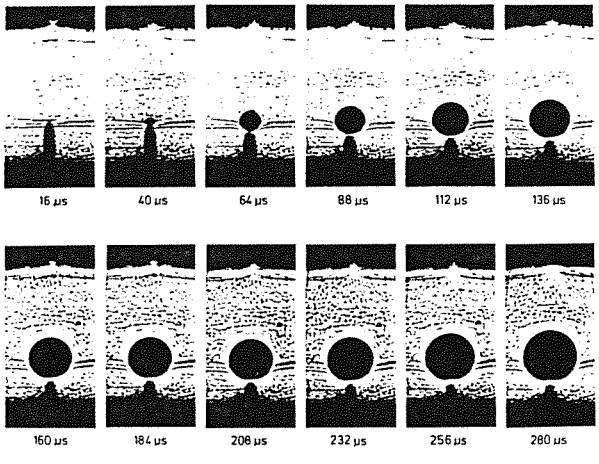

Fig. 15. Crack tip caustics under drop weight loading (photographed in reflection with a high strength steel specimen)

the striking hammer measure the load during impact. The impact fracture toughness is derived from the critical value of the load the specimen is subjected to for the moment of crack initiation. Recommended procedures for performing the test and for evaluating the data are given in [8].

4.1 Dynamic Behaviour of Impacted Cracks

The mechanical behaviour of cracks under impact loading was investigated by measuring the dynamic stress intensity factors directly at the crack tip by means of the shadow optical method of caustics [6,9]. Specimens of Araldite B and of a high strength steel were investigated. Figure 14 gives a schematic view of the experimental set-up showing the shadow optical arrangement in reflection with a high strength steel specimen. The influence of dynamic effects was evaluated by comparing the dynamic stress intensity factors, K_I^{dyn}, with equivalent static stress intensity factors, K_I^{stat}. The static values were determined from the measured hammer load P_H utilizing conventional static stress intensity factor formulas from ASTM E 399.

A series of twelve shadow optical photographs of the central part of an impacted steel specimen is shown in Fig. 15. Quantitative data for the two materials Araldite B and a high strength steel are given in Fig. 16. The specimens were impacted at a velocity of 0.5 m/s by a hammer of mass 4.9 kg or 90 kg respectively. The dynamic stress intensity factors K_I^{dyn} (experimental points) and the corresponding static stress intensity factors K_I^{stat} (thin curves) are plotted as functions of

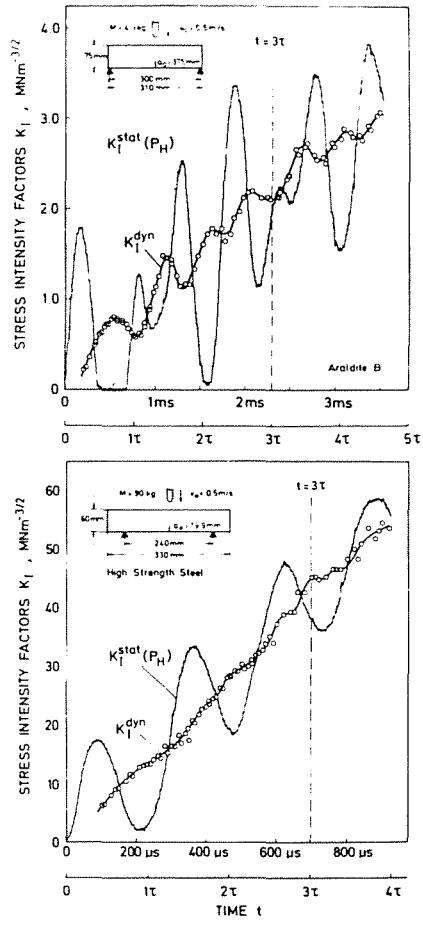

Fig. 16. Stress intensity factors for cracks under drop weight loading a) Araldite B specimen, b) high strength steel specimen

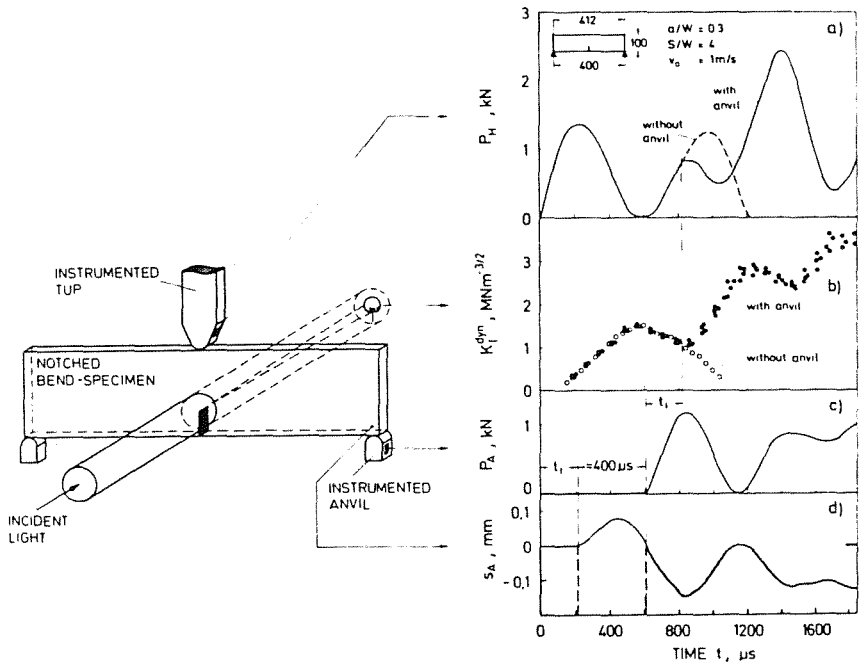

Fig. 17. Mechanical response of a notched bend specimen to drop weight loading

time. The times are given in absolute units and also in relative units by normalization by the period τ of the eigenoscillation of the impacted specimen.

The K_I^{stat} -values show a strongly oscillating behaviour, whereas the actual dynamic stress intensity factor K_I^{dyn} show a more steadily increasing tendency. In the early time range, $t < \tau$, these differences are very pronounced. The differences become smaller with increasing time, but even for times larger than 3τ the influence of dynamic effects obviously has not vanished and there are still marked differences between K_I^{stat} and K_I^{dyn}. Due to the different contact stiffnesses the effects are larger with Araldite B than with high strength steel.

4.2 Reaction of the Specimen to Impact Loading

The behaviour of specimens under impact loading was further investigated by also measuring the specimen reaction at the anvils [6]. Figure 17 compares the load measured at the striking hammer (a), the stress intensity factor measured at the crack tip (b), the load measured at the anvils (c), and the position of the specimen ends with regard to the anvils (d). The data were obtained with Araldite B specimens impacted at 1m/s. The τ-value of the specimens utilized for these investigations is about 700 µs. A comparison of the four signals indicates that non-zero loads at the anvils are registered only after a rather long time of about 600 µs. This time is about three times larger than the time it would take the slowest wave, i.e. a transverse wave, to travel from the point of impact to the anvils. This unexpected behaviour is explained by diagram (d) in Fig. 17. A loss of contact is observed between the specimen ends and the anvils. The loss of contact starts at about 200 µs. This time is in agreement with the above consideration of wave propagation times. For about the next 400 µs the specimen is completely free and only after this time, i.e. at a time of about 600 µs total, do the specimen ends come into contact again with the anvils. In accordance with this observation loads are then recorded at the anvils. With different test conditions this loss of contact can occur later for a second time and loss of contact can also take place between the hammer and the specimen.

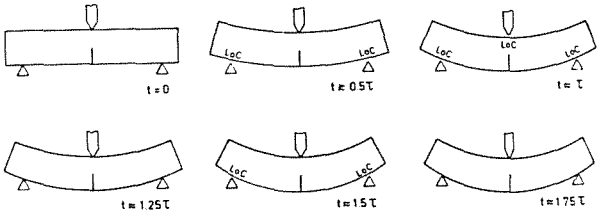

Fig. 18. Loss-of-contact (LoC) effects observed with impacted specimens

These processes are illustrated by the schematic representation in Fig. 18. Since in these experiments, the anvils were obviously of no influence during the early phase of the impact process, additional experiments were performed with unsupported specimens. The results are represented by the dashed curve and open data points in Fig. 17. In accordance with speculation, the early specimen reaction ($t < \tau$) is the same for both, the supported and the unsupported specimen.

4.3 Validity of Impact Fracture Toughnesses K_{Id}

The data demonstrate the strong influence of dynamic effects on the mechanical behaviour of cracks under

impact loading. The method [8] proposed to ASTM for measuring the dynamic fracture toughness K_{Id} in instrumented impact tests assumes that for times larger than 3τ, K_I^{stat}-values would represent a good approximation of the actual dynamic stress intensity factor K_I^{dyn}. However, data from the presented experiments indicate that a static analysis is not at all adequate to describe the loading condition in the specimen under the proposed conditions, except at much later times, i.e. for $t/\tau >> 3$. Large times-to-fracture t_f result for high test temperatures and small impact velocities. Small τ-values, on the other hand, result for small specimen dimensions. Often t_f and τ, however, cannot be varied independently due to size requirements which in general demand large specimen dimensions for high test temperatures. In order to overcome these difficulties as well as the resulting restrictions on the choice of test parameters a fully dynamic measuring procedure, the socalled method of impact response curves, has been developed by the author and his colleagues, for details see [10]. This concept of impact response curves allows to correctly determine impact fracture toughnesses K_{Id} under arbitrary test conditions, even under test conditions that result in extremely high rates of loading.

6. SUMMARY AND CONCLUSION

The shadow optical method of caustics for determining stress intensity factors from the actual stress strain field around the tip of a crack tip is presented. The method is used in combination with high speed photography to investigate the influence of dynamic effects on test procedures for measuring dynamic fracture toughnesses. The crack arrest toughness K_{Ia} and the impact fracture toughness K_{Id} are considered as examples. For arresting cracks the stress condition at arrest is found to be still dynamic and not static although the crack velocity has become zero. The dynamic effects become small for small crack propagation velocities only. For cracks under impact loading conditions the stress intensity factors cannot be adequately derived from measured load values via static evaluation procedures. Only for large times to failure, as they result for small impact velocities and/or ductile material behaviour, do static approaches represent acceptable approximations. Reliable crack arrest and impact fracture toughnesses can only be obtained by evaluation procedures which take the dynamic effects into account. In general, the observed findings demonstrate that it can be very misleading to apply knowledge based on quasi-static fracture processes to dynamic situations. An appropriate consideration of the relevant time effects is needed for a successful treatment of dynamic fracture problems. Only on the basis of such fully dynamic investigations can one make decisions on the validity range of quasi-static measuring procedures or on the necessity for the application of fully dynamic test procedures.

7. REFERENCES

[1] Manogg P., "Anwendung der Schattenoptik zur Untersuchung des Zerreissvorgangs von Platten", Dissertation, Universität Freiburg, Germany, (1964)

[2] Kalthoff J.F., "Shadow Optical Method of Caustics", Chapter 9 in "Handbook on Experimental Mechanics", Ed. A.S. Kobayashi, Second Revised Edition, VCH Publishers, New York, 407-476 (1993)

[3] Theocaris P.S., "Complex Stress Intensity Factors of Bifurcation Cracks", J. Mech. Phys. Solids 20, 265-279 (1972)

[4] Rosakis A.J., Ma C.C., Freund L.B., "Analysis of the Optical Shadow Spot Method for a Tensile Crack in a Power-Law Handening Material", J. Appl. Mech. 50, 777-782 (1983)

[5] ASTM E 1221, "Standard Test Method for Determining Plane-Strain Crack-Arrest Toughness, K_{Ia}, of Ferritic Steels", American Society for Testing and Materials, Philadelphia (1996)

[6] Kalthoff J.F., "On the Measurement of Dynamic Fracture Toughnesses - A Review of Recent Work", Int. Journ. of Fracture 27, "Special Issue on Dynamic Fracture", 277-298 (1985)

[7] Kalthoff J.F., Beinert J., Winkler S., "Measurements of Dynamic Stress Intensity Factors for Fast Running and Arresting Cracks in Double-Cantilever-Beam Specimens", Fast Fracture and Crack Arrest, ASTM STP 627, Eds., Hahn G.T. and Kanninen M.F., American Society for Testing and Materials, Philadelphia, 161-176 (1977)

[8] ASTM E 24.03.03, "Proposed Standard Method of Test for Instrumented Impact Testing of Precracked Charpy Spcimens of Metallic Materials", Draft 2d, American Society for Testing and Materials, Philadelphia (1981)

[9] Kalthoff J.F., Böhme W., Winkler S., "Analysis of Impact Fracture Phenomena by Means of the Shadow Optical Method of Caustics", Proc. VIIth Int. Conf. on Experimental Stress Analysis, organized by SESA, Haifa, Israel, Aug. 23-27, 148-160 (1982)

[10] Kalthoff J.F., Winkler S., Böhme W., "A Novel Procedure for Measuring the Impact Fracture Toughness K_{Id} with Precracked Charpy Specimens ", Proc. Int. Conf. on Mechanical and Physical Behavior of Materials under Dynamic Loading, Paris, Sept. 2-5, 1985, Journal de Physique, Colloque C5, supplément n° 8, Thome 46, 179-186 (1985)